Pergamon

Deep-Sea Research II, Vol. 44, No. 9–10, pp. 1783–1800, 1997

Printed in Great Britain

PII: S0967–0645(97)00023–4

0967–0645/98 $19.00+0.00

Physical and nutrient variability in the upper equatorial Pacific associated with westerly wind forcing and wave activity in October 1994

GÉRARD ELDIN, MARTINE RODIER and MARIE-HÉLÈNE RADENAC

(*Received in revised form* 17 *March* 1997; *accepted* 21 *May* 1997)

Abstract—In September–October. 1994, the FLUPAC cruise was carried out in the western equatorial Pacific as a French contribution to the JGOFS programme. One leg of that cruise included a zonal transect along the equator, from 170°E to 150°W. Physical and nutrient data from that section presented unusual features: zonal currents in the upper layer were mostly found in opposition to local forcing, i.e. westerly winds and westward flow west of 180°, easterly trade winds and weakly eastward flow elsewhere; east of 170°W strong oscillations of the meridional flow (0.8 m s^{-1} peak to peak) extended from the surface to the thermocline; a warm (higher than 30°C), fresh ($S<34.8$) and salinity-stratified surface water mass spread out from 170°E to 172°W, where it ended through a salinity front; east of that limit a deep homogeneous layer was found, but with relatively low vertical mixing; the thermocline deepened steadily from 170°E eastward to a depth of 160 m at 160°W; the boundary of nutrient enriched waters was displaced by about 2800 km eastward as compared with climatology, with 1 μM surface NO_3 concentration at 165°W; a relative nutrient minimum (less than 3 μM NO_3) was found embedded in the enriched area east of that longitude. These observations are explained with the help of large-scale data from the TAO mooring array: 61 days of westerly winds in the western Pacific before the cruise had triggered a 0.4 m s^{-1} current jet that advected surface waters to the east; a downwelling Kelvin wave propagated east of that wind patch, depressed the thermocline, and changed geostrophic surface current to eastward; tropical instability wave activity caused localized nutrient depletion by meridional advection; west of 180°, propagation of an upwelling Rossby wave from the east may have contributed to westward flow. These results stress the importance of intraseasonal variability on physical and nutrient content data obtained during a cruise, and the usefulness of concurrent large-scale observations.

INTRODUCTION

In the western and central equatorial Pacific Ocean, the largest variability in the physical structure of the upper layers is associated with interannual signals, namely the El Niño–Southern Oscillation (ENSO) cycle (e.g. Kessler and Taft, 1987; McPhaden *et al.*, 1990; Delcroix *et al.*, 1992). Influence of the interannual, ENSO-related, variability on nutrient distribution and primary production has been studied in the western Pacific, mostly at 165°E (Blanchot *et al.*, 1992; Dandonneau, 1992; Le Bouteiller *et al.*, 1992; Radenac and Rodier, 1996). In this region, warm phases of ENSO are characterized by a shoaling of the thermocline and nitracline. Surface values are dictated by the western extension of the equatorial cold tongue, which reaches 165°E only during strong cold ENSO episodes. In the

ORSTOM, BP A5, 98848 Nouméa , New Caledonia.

eastern Pacific, deepening of the nitracline and depletion of surface waters are linked to the decrease or disappearance of upwelling during warm phases (e.g. Feely *et al.*, 1987; Barber and Kogelschatz, 1990). Recently, the US–JGOFS EqPac process study (JGOFS, 1990) was able to sample mature El Niño and more "normal" conditions in the central Pacific (Murray *et al.*, 1994): from September 1991 to March 1992, a series of westerly wind events in the western Pacific triggered several Kelvin waves that propagated eastward and caused depression of the thermocline and nutrient depletion of surface waters at 140°W. Results from that study stressed the importance of remote physical processes in controlling nutrient content and biological processes in the central Pacific on time-scales of several months.

At shorter time-scales, intraseasonal variations in surface forcing also can have a strong impact on the physics of the surface equatorial layer. Historically, propagation of equatorial Kelvin waves were mostly observed during periods of El Niño onset or mature phase (Enfield, 1987). These phenomena are actually much more frequent and, although their effects extend further east during El Niño events, the central Pacific is continuously affected by individual propagative events (Kessler *et al.*, 1995). Effects of these isolated events on the physical structure of the western Pacific are now well known (e.g. McPhaden *et al.*, 1988; Delcroix *et al.*, 1991, 1993), and the effects of a strong wind burst on meridional NO_3 concentration were described by Radenac and Rodier (1996).

A cruise through the equatorial Pacific in September–October 1994 gave another opportunity to study the variability in physical and nutrient structure along the equator associated with a strong westerly wind burst and the propagation of equatorial waves. The purpose of this paper is to explain observations from that cruise in relation to local and atmospheric forcing through several different physical mechanisms.

DATA

The data used in this study were mostly collected during the FLUPAC cruise, carried out through the tropical Pacific from 23 September to 29 October 1994, as part of the French contribution to the international JGOFS programme. That cruise included several sections and fixed stations, but only data from the equatorial leg will be used here. That zonal transect was conducted from 170°E to 150°W, on 9–18 October 1994. Along the section, 21 stations provided 0–1000 dbar CTD casts and water samples for nutrient and other analyses. Vertical profiles of temperature and salinity were processed to a 2 dbar vertical resolution from observations made with a SeaBird SBE-911*plus* CTD, and final values validated after laboratory calibrations of sensors. Samples from about 12 levels in the first 200 dbar were collected for nutrients: nitrate (NO_3), phosphate (PO_4), and silicate (SiO_3) were immediately analysed at sea with a Technicon Autoanalyzer II, using standard colorimetric methods described by Strickland and Parsons (1972). For NO_3 concentrations lower than 1.5 μM, the high sensitivity (HS) method described by Oudot and Montel (1988) was applied. The lower limits of detection of the various analyses are: 0.003 μM for NO_3 (HS method), 0.01 μM for PO_4, and 0.05 μM for SiO_3. Routine analytical procedures have been described by Bonnet (1995).

Continuous records of upper ocean currents were obtained during the cruise from the simultaneous use of two RD Instruments ADCPs, a long-range 75 kHz model with a vertical resolution of 16 m and first data bin centred at 28 m, and a short-range 300 kHz instrument of 4 m vertical resolution with first bin at 12 m. Velocity data were averaged in 5 min ensembles for both instruments. Before the cruise, absence of interference between the

two instruments was carefully checked. The two data sets were processed separately using the CODAS3 software (e.g. Bahr *et al.*, 1989). Absolute velocities obtained with help of GPS navigation showed less than 5 cm s^{-1} r.m.s. difference at common depth levels for the two ADCPs in the first 100 m, so that both data sets could be merged to provide vertical profiles from 12 to 700 m on average. Details on data processing and other observations from the FLUPAC cruise can be found in the cruise report (Le Borgne *et al.*, 1995).

To place the cruise in the large-scale context of the equatorial Pacific, data from the TAO (Tropical Atmosphere Ocean) buoy array also will be used, including thermistor chain and currentmeter buoys (e.g. McPhaden *et al.*, 1990). These data are distributed by the TAO Project Office, NOAA, Seattle, WA, USA. Daily averaged wind and ocean current observations from the 0°–165°E mooring and time–longitude plots of derived products along the equator will be presented.

CRUISE OBSERVATIONS

Wind forcing and velocity fields

This study will focus on the upper layers of the equatorial Pacific, where variability associated with external forcing is strongest. The following description will therefore be restricted to layers in and above the thermocline, above 250 dbar. Figure 1 presents wind vectors measured along the ship path and vertical sections of the two components of currents. West of the date-line, southwesterly to westerly winds of 3–5 m s^{-1} were encountered during the first 4 days of the section (Fig. 1a). At this time of year, winds are expected to be easterlies in this area, except during periods of warm anomalies (Kessler *et al.*, 1995). East of the Date Line, as the cruise proceeded eastward, trade winds appeared and increased progressively to 7–8 m s^{-1} east of 160°W, while veering to the south-east.

A plot of current vectors in the upper oceanic mixed layer, roughly above 40 m (Fig. 1b) emphasizes a rich small-scale zonal structure with strong zonal shear of meridional velocity. The zonal component was strongly westward (0.4 m s^{-1}) in this layer only west of the Date Line, and flow was mainly eastward (0.2 m s^{-1}) between 180 and 172°W. From that longitude to 150°W, the meridional component dominated the equatorial surface flow, with meridional velocities of the order of 0.25 m s^{-1}, more than twice the zonal velocity, which stayed weakly eastward (0.1 m s^{-1}) on average. These meridional currents were composed of bands of alternative northward and southward flows, 200–500 km wide and 800–1000 km apart. The southward band around 163°W was very weak, but the vertical section confirms its existence (Fig. 1d). These observations contrast with previous measurements in the area, where the westward flowing South Equatorial Current (SEC) was generally well defined (Wilson and Leetmaa, 1988; Eldin *et al.*, 1992). Also, this surface flow was not obviously related to local wind forcing: west of the Date Line, local wind and zonal current were of opposite directions; east of the Date Line the pattern was more complex, but local wind and surface current were not related either, except around 158–154°W where trade winds were above 5 m s^{-1}, and zonal flow slightly westward. This behaviour was different from what had often been observed west of 170°E, where upper layer circulation was found to adjust quickly to changes in the local wind forcing on the equator (Delcroix *et al.*, 1993; Eldin *et al.*, 1994).

Below 50–60 m, the vertical sections of zonal velocity (Fig. 1c) show a more classical picture: the SEC presented a velocity maximum around 100 m, always above 0.5 m s^{-1} west

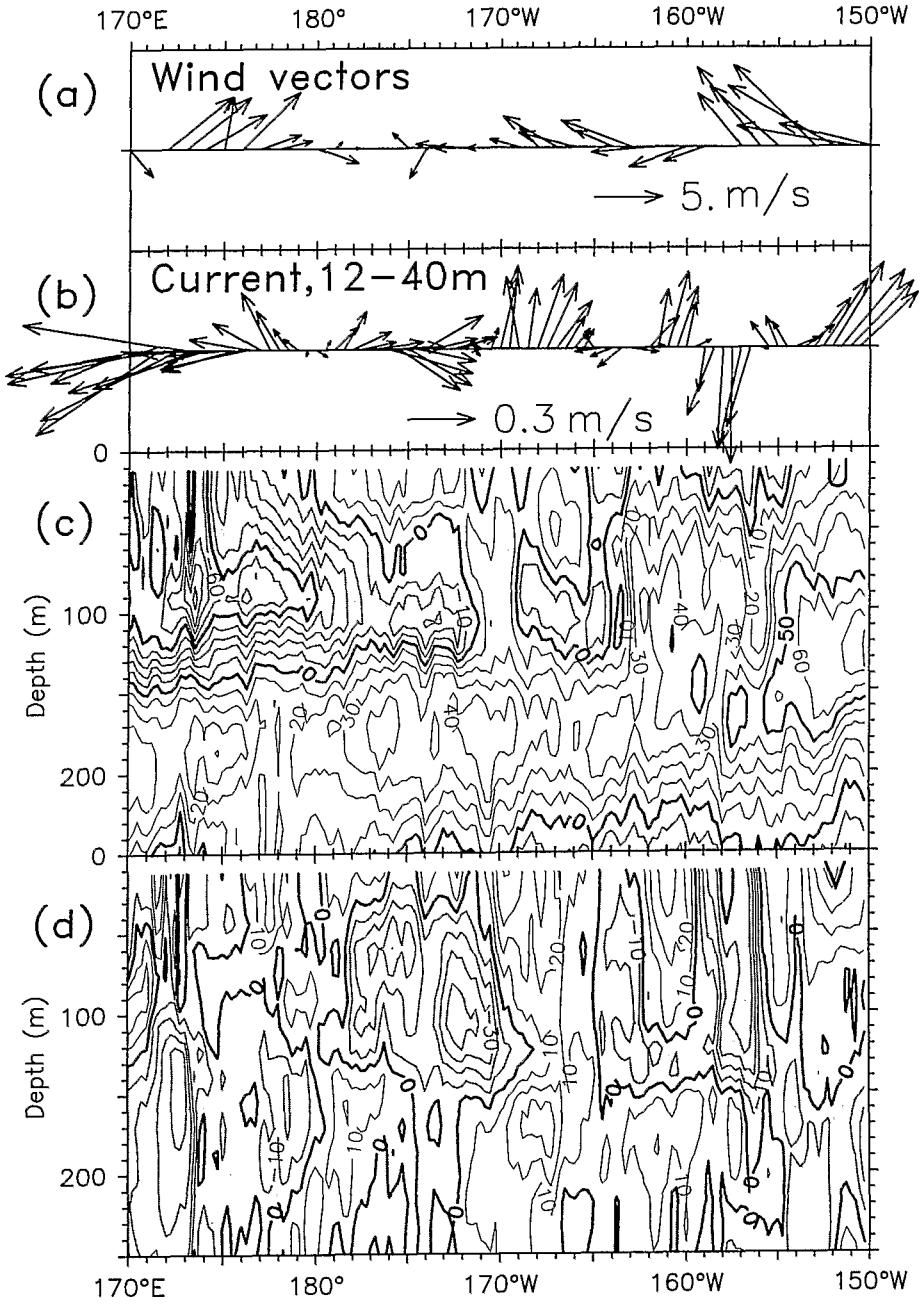

Fig. 1. Results from the FLUPAC cruise equatorial leg, 9–18 October 1994: (a) wind vectors obtained from observations on the ship's bridge; (b) ADCP current vectors in the surface layer 12–40 m; (c) zonal current sections; (d) meridional current sections. Isolines are drawn every 0.1 m s^{-1}, with westward and southward components shaded.

of 180°, which gradually weakened to 172°W. There, zonal current reversed and the whole water column turned eastward for about 300 km. From 169–163°W a weak SEC reappeared (0.1 m s^{-1}). The Equatorial Undercurrent (EUC) appeared below, about 100 m thick, with a velocity core of 0.35 m s^{-1} centred at 200 m, slightly shallowing to 180 m at 163°W, and a small increase in zonal velocity to about 0.4 m s^{-1}. East of that longitude the eastward flow stretched vertically and took up the whole 0–200 m depth layer, except for a small area in surface around 156°W, as noted above. The core of the EUC also shoaled in steps, and rose to 120 m at 155°W and eastward; its velocity increased abruptly, reached 0.5 m s^{-1} at 155°W but merely passed 0.8 m s^{-1} at 150°W. These figures of EUC velocities are lower than most previous observations in the area. At 165°E TAO mooring data gave an average EUC core speed of 0.47 m s^{-1} for the period January 1986–January 1992 (McCarty and McPhaden, 1993). In the eastern part of our section, results from an equatorial mooring at 170°W (Weisberg and Hayes, 1995) showed an average EUC velocity of 0.65 m s^{-1}. Most observation programmes between 150°W and 160°W, like the Hawaii to Tahiti Shuttle Experiment (Johnson and Luther, 1994) or the Line Islands Profiling Programme (Firing, 1987), led to average EUC core velocities of more than 0.7 m s^{-1} for 16 month averages.

On the meridional velocity section (Fig. 1d), the area at the onset of the transect presented some fine-scale features included in the SEC. A broad band of southward flow reaching 0.4 m s^{-1} deflected the SEC between 180° and 170°W. To the east, the strong meridional oscillations described in the upper layer (Fig. 1a) extended downward to the upper part of the EUC, at 120–150 m. Below that depth, meridional components were mostly northward, but weak (0.1 m s^{-1}).

Temperature and salinity

Temperature and salinity sections are presented in Fig. 2. The most prominent feature in upper ocean waters was the appearance of a very warm (higher than 30°C) and fresh water mass in the western half of the section. The 30°C isotherm and the $S=35.0$ isohaline closely matched, from 172°E to 170°W, the easternmost limit of the 30°C water. Whereas this water mass was very homogeneous in temperature, almost entirely between 30.0 and 30.5°C, it was vertically stratified in salinity and was bounded to the east by a salinity gradient at 174–170°W. In fact, data from the ship thermosalinograph (not shown) exhibited a sharp salinity front at the surface ($\Delta S = +0.4$ over a distance of 40 km, with the last +0.2 over 2 km) at 172°W. A similar combination of high-temperature–stratified-salinity pool of water had been observed in the area during a Japanese cruise in January–February 1990 (Kuroda and McPhaden, 1993), but with the salinity front around 178°E. In that study, the maximum temperature was lower by 1°C and surface salinity higher by +0.5 than in our observations. This water mass was almost entirely flowing eastward, whereas, in our case, only a small region above 50 m depth was doing so (Fig. 1c).

Within this warm pool region, a small area centred at 176°E of 29.7°C temperature and $S=33.7$ salinity was associated with strong local rainfall, as experienced during the cruise. Further east, the water layer of temperature above 28°C extended to 156°W, and even slightly deepened, from 100 m at 170°E to 120 m at 160°W. On the eastern side of the $S=35.0$ salinity front in the upper layer, the vertical salinity stratification disappeared and values kept between $S=35.0$ and 35.3 almost everywhere above the thermocline, except in a small area centred at 165°W. Around 160–163°W opposite salinity and temperature intrusions intermingled from 20 m down to the thermocline (Fig. 2b).

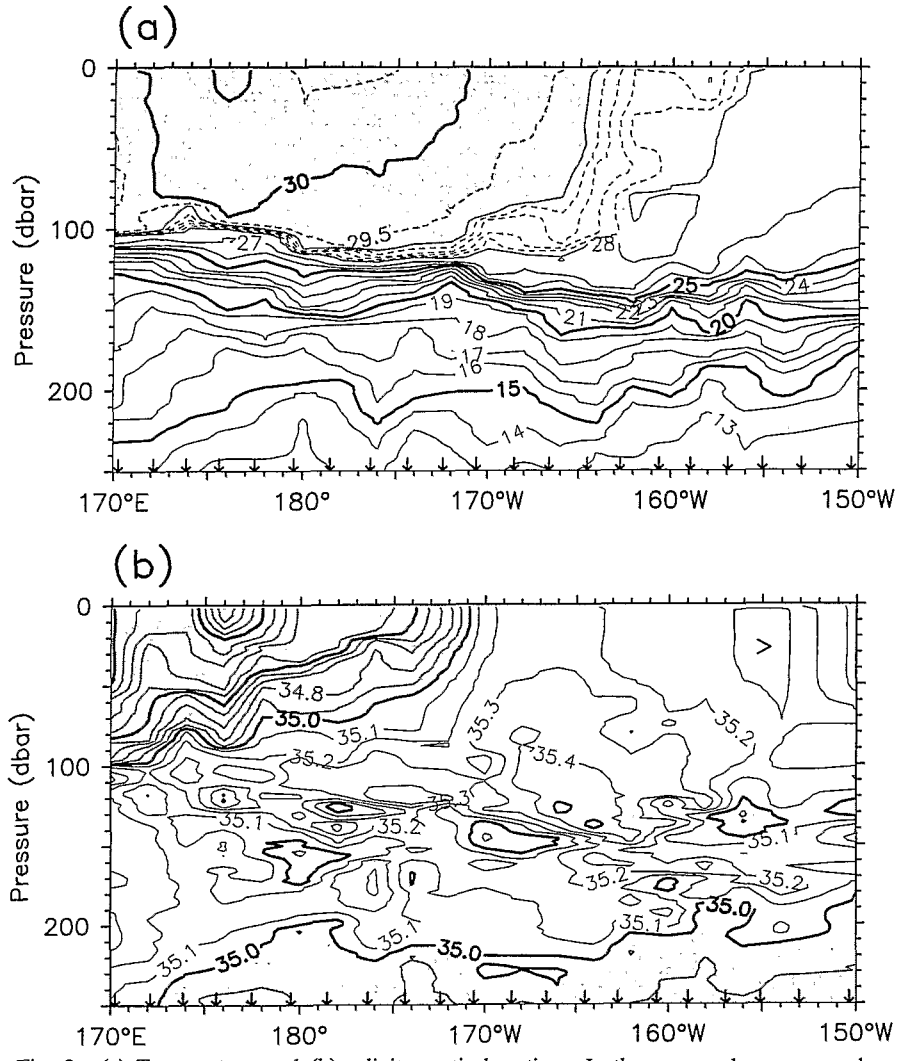

Fig. 2. (a) Temperature and (b) salinity vertical sections. Isotherms are drawn every degree centigrade, and isohalines every 0.1 psu. Temperatures isolines 28.2°C to 28.8°C and 29.5°C are shown to highlight fine structure in the upper layer (dashed). Temperatures above 29°C and salinities under 35.0 psu are shaded. Station locations are shown by small arrows at bottom of plots.

Below that warm layer, the upper thermocline (isotherms 20–25°C) steadily deepened from 120 m at 170°E to 150 m at 162°W, and then spread and rose by about 10 m. Such downward slope toward the east of the upper thermocline above the upward slope of deeper isotherms had been previously observed in the region, but was generally confined at or west of 180° (e.g. Halpern, 1980; Mangum *et al.*, 1990; Eldin *et al.*, 1992). At these depths the general envelope of the salinity distribution followed the thermocline, but the fine-scale salinity structure was complicated: this is the northern limit of the high-salinity tongue of Tropical Water (Tsuchiya *et al.*, 1989), which ends with a meridional gradient across the

equator. Below 200 m, vertical fluctuations at the base of that tongue were closely associated to vertical displacements of water masses delineated by the 14°C and $S = 35.0$ isolines. This was most notable at 177°E, 172°W and 157°W.

To determine how FLUPAC data differ from the "normal" state of the equatorial Pacific, we compared our results with existing climatologies. For this purpose, we used the recently issued *World Ocean Atlas* of NOAA (Conkright *et al.*, 1994). This atlas provides monthly and annual climatologies for temperature and salinity, and annual climatologies for nutrients. FLUPAC temperatures are comparable with October averages, but monthly salinity averages are not complete for the region; because of a lack of historical data, annual values will be used instead, as for nutrients in a following paragraph. Focus will be given to surface anomalies (0–10 m, Fig. 3a) and to anomalies in the upper thermocline (Fig. 3b). As expected, surface temperatures were everywhere above the October average. Positive anomalies were higher in the west, about +1.7°C, and reached a maximum of +2°C around 168°W. In the east the average anomaly was +1.2°C. Fine-scale events were noticeable, such as the rain-induced surface cooling at 176°E, and the local, probably advective warming at 157–162°W. Whereas surface salinity was close to normal in the east, it was about 1 below normal to the west of the salinity front; here also the rain event at 176°E was evidenced. The 25°C isotherm was 15 m too shallow west of the Date Line, and the depth anomaly steadily increased to 30 m at 150°W. This confirms the reversal of the zonal thermocline slope along the equator.

Vertical mixing

Clearly, the very different hydrological structures encountered along the ship path and their anomalous values will affect the distribution of nutrients. This effect can be evaluated by an estimation of the different terms that play a role in vertical mixing, namely, density stratification and vertical velocity shear. However, quantitative estimates of mixing rates

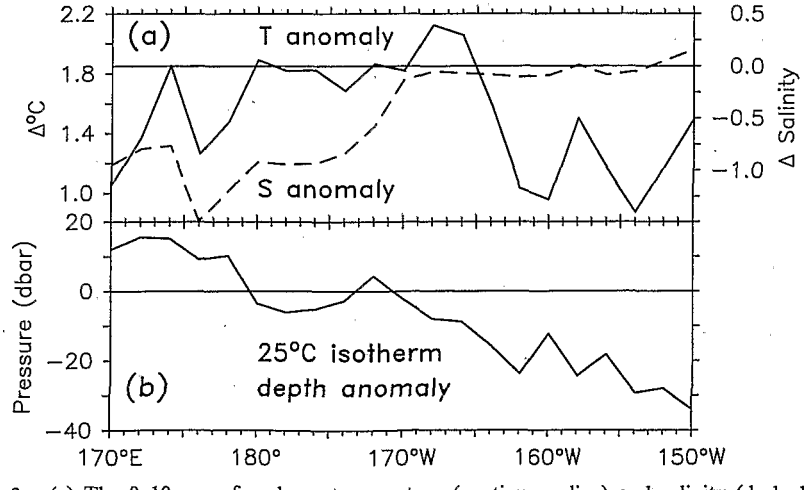

Fig. 3. (a) The 0–10 m surface layer temperature (continuous line) and salinity (dashed line) anomaly; (b) the 25°C isotherm depth anomaly. Climatology was provided by the *NOAA World Ocean Atlas 1994*.

along the cruise track will not be possible, because of a lack of specific turbulence measurements.

Density stratification is expressed through the buoyancy frequency N (Fig. 4a). As usual, this parameter reached its maximum in the upper thermocline, with values of more than $0.02\ s^{-1}$ in a 30 m thick layer. It decreased in the underlying layer to less than $0.01\ s^{-1}$ below the high-salinity tongue. Above the high stratification layer, two regions were present along the transect: west of the salinity front at 172°W, N^2 was generally in the range of 1×10^{-4} to $2 \times 10^{-4}\ s^{-2}$ whereas east of the front N^2 remained lower than $1 \times 10^{-4}\ s^{-2}$. Following the gradient criteria of Lukas and Lindstrom (1991), the mixed layer depth is defined as the first depth where the density gradient exceeds $0.01\ kg\ m^{-4}$ and the depth of the top of the thermocline is the first depth where the temperature gradient exceeds $0.05°C\ m^{-1}$; a large difference between these two depths (plotted in Fig. 4) would be caused by salinity stratification, which acts as a barrier layer and reduces vertical exchanges. West of the salinity front, the mixed layer depth fluctuated between 20 and 40 m and the top of the thermocline was located between 70 and 100 m, resulting in a 40–90 m thick barrier layer. Conversely, there was no barrier layer east of the salinity front because of the coincident deepening of the mixed layer depth and the top of the thermocline to 90–120 m. An exception was found in the already noted small area of surface warming around 157–158°W. N^2 was lower than $1 \times 10^{-4}\ s^{-2}$ in the mixed layer and between 1×10^{-4} and $2 \times 10^{-4}\ s^{-2}$ in the barrier layer.

The structure of the squared vertical shear $Sh^2 = (\partial u/\partial z)^2 + (\partial v/\partial z)^2$ calculated over a vertical scale of 16 m (Fig. 4b) was reminiscent of the buoyancy frequency structure in Fig. 4(a). The EUC is a region of weak shear ($Sh^2 < 10^{-4}\ s^{-2}$) and, most of the time, the minimum value was situated at the core level. It was usually deeper than the highly density-stratified layer, except east of 160°W, where the EUC core was coincident with the upper thermocline. Above the EUC, the depths of maximum shear closely followed the depth of maximum buoyancy frequency. Hence, vertical shear in the western part of the transect ($Sh^2 > 4 \times 10^{-4}\ s^{-2}$) was stronger than east of the front. East of 170°W, the maximum values of the total shear squared barely exceeded $2 \times 10^{-4}\ s^{-2}$ and were lower than previously reported values: about $4 \times 10^{-3}\ s^{-2}$ at 140°W (Peters *et al.*, 1991) or at 150°W (Carr *et al.*, 1992). In that eastern region, contribution of the meridional component to the total shear was significantly larger than west of the front (Fig. 4c).

Because of similar spatial distributions of density stratification and vertical shear, the Richardson number ($Ri = N^2/Sh^2$) computed on a 16 m vertical scale did not have significantly different values between the western and eastern parts of the transect, with values of order unity (moderately turbulent regime) above the EUC (higher Ri were found in the EUC). Typical profiles of Ri west of the front were relatively consistent with the mean profile of Ri presented by Wijesekera and Gregg (1996) in the western Pacific warm pool. East of the front, despite reduced static stability and because of lower than usual vertical shear, Ri values of order unity were also measured whereas values of much less than unity (highly turbulent regime) are usually reported in that area (Peters *et al.*, 1991; Carr *et al.*, 1992; Lien *et al.*, 1995). Indeed, also in terms of vertical mixing, hydrological and current regimes east of the salinity front led to anomalous results.

Nutrients

Nitrate, phosphate, and silicate distributions along the equator are shown in Fig. 5. In the

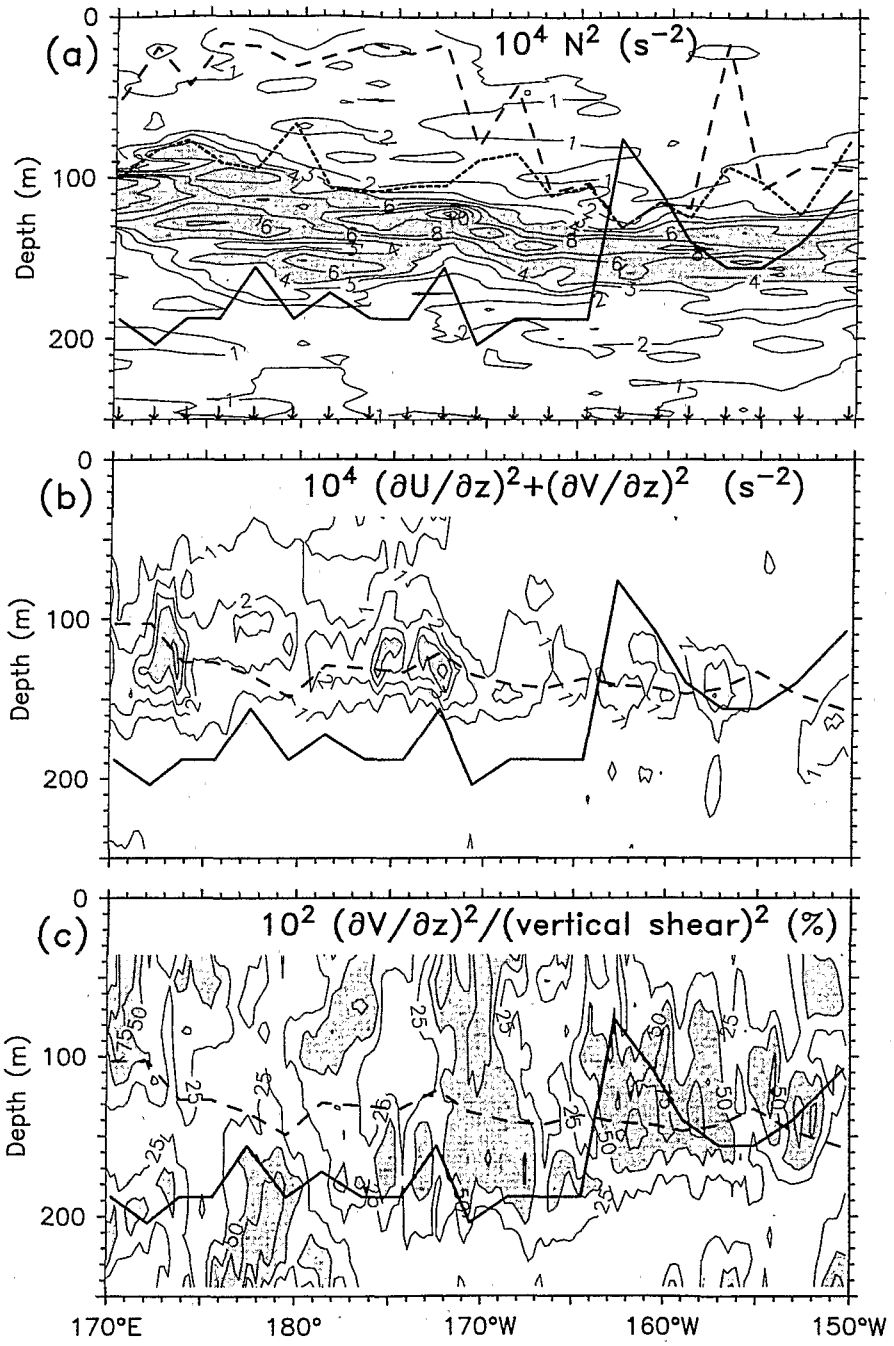

Fig. 4. Vertical sections of (a) density stratification N^2, (b) vertical velocity shear squared Sh^2 and (c) percentage of meridional shear in Sh^2. On the three panels the depth of the maximum eastward flow is plotted (continuous line). In (a), depth of the density mixed layer (dashed line) and depth of the top of the thermocline (dotted line) are shown. In (b) and (c), depth of maximum stratification is plotted (dashed line).

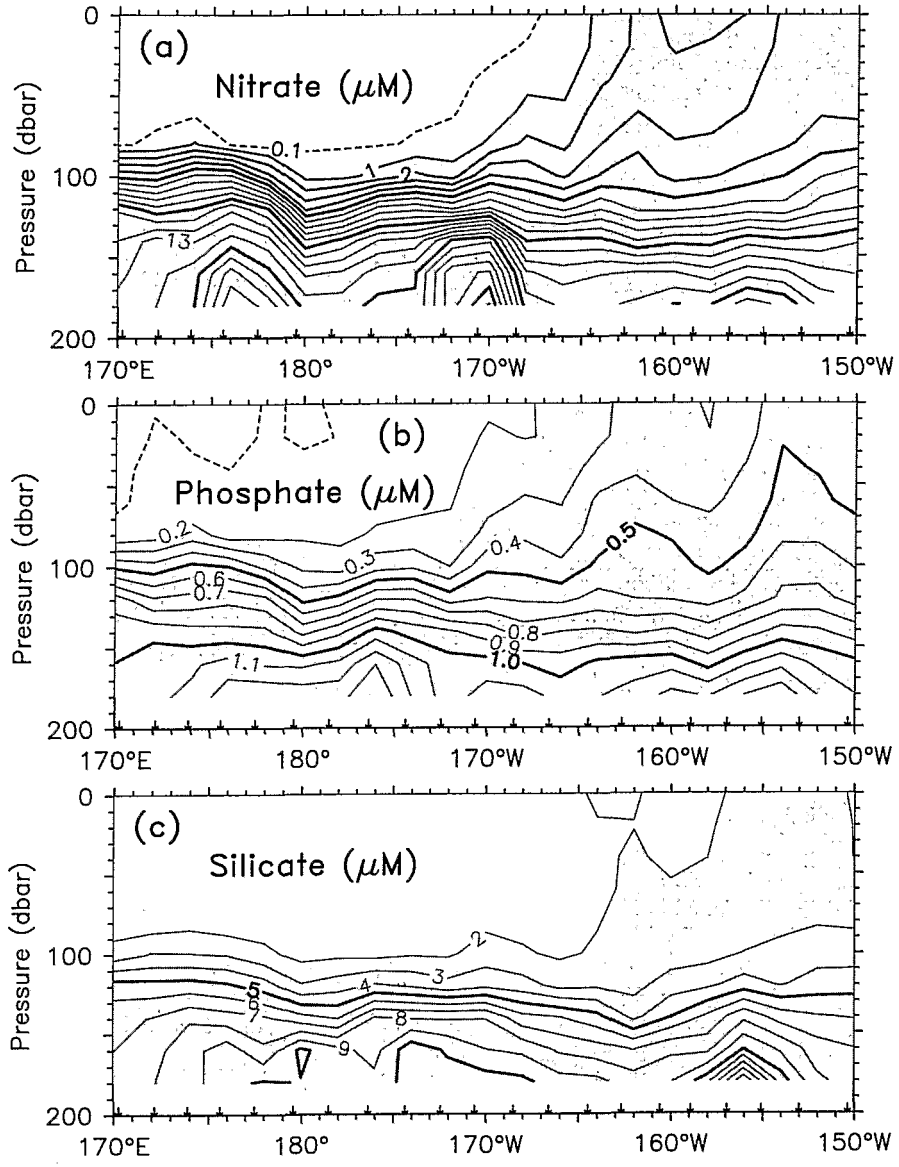

Fig. 5. (a) Nitrate, (b) phosphate and (c) silicate vertical sections. Isolines are drawn every 1 μM, 0.1 μM, and 1 μM, respectively. The 0.1 μM isoline of nitrate is added (dashed).

western part of the transect, nitrate was generally undetectable (less than 0.005 μM) in surface waters, whereas phosphate and silicate were always found at concentrations of about 0.15 μM and 1.5 μM, respectively. These nutrient concentrations are characteristic of an oligotrophic regime and very similar to the conditions described in the western equatorial Pacific in non-ENSO conditions at 155°E (Mackey *et al.*, 1995) or 165°E (Radenac and Rodier, 1996). Nitrate-depleted waters extended down to 80–90 m and coincided with the previously defined warm and salinity-stratified water mass. The top of the nitracline (as

defined by the 0.1 μM isoline) was below the barrier layer. Thus, surface waters were dynamically isolated from the nitracline, as observed in the extreme western Pacific (Mackey *et al.*, 1995). The eastward extension of nutrient-poor waters was bounded by the salinity front surfacing at 172°W. However, in the near-surface layer, no nitrate was detected before 168°W. We hypothesize that this surface depletion in part may result from biological nitrate removal.

East of 168°W in the upper layer, surface nitrate concentrations increased progressively eastward, as temperature decreased, and reached 3.26 μM in surface layers at 150°W. Phosphate and silicate extrema were also found at 150°W (0.45 μM and 2.6 μM, respectively). These figures represent relatively high nutrient content for surface waters at more than 27°C. However, the area cannot be considered as "nutrient rich", according to Barber and Chavez (1983), who defined such waters with nitrate content above 4 μM. Other distinctive features of nutrient distributions in the eastern region of the transect were the minima observed between 162°W and 156°W for nitrate, phosphate and silicate. These minima were detectable down to about 100 m, as shown by the deepening of the isolines, and were associated with the patch of surface water with relatively high temperature (higher than 28.4°C) and low salinity ($S<35.2$) seen in Fig. 2.

At depth, nitrate concentrations increased in the upper thermocline and high values (greater than 10 μM) were observed below the thermocline. The nitracline was shallowest at 170°E and deepened eastward. After 162°W, the nitracline rose by about 20 m, following the thermocline. The slopes of the deep nitrate isolines and thermocline isotherms coincided. Nitrate vertical gradient within the nitracline was particularly sharp (0.2–0.3 μM m^{-1}) under the depleted water mass in the west. East of the front, isolines in the nitracline spread, decreasing the vertical gradient to about 0.1 μM m^{-1}. Identical features were present in phosphate and silicate distributions, with minor differences. Below 150 m, there were domings of nutrient concentrations isolines, at 177°E, 172°W and 157°W, which were well marked in terms of nitrate. These features were consistent with, but did not perfectly match, vertical displacements of nutrient-rich deeper waters suggested by corresponding features in temperature and salinity data (Fig. 2).

The western region may be viewed as a two-layer system in which a nutrient-poor oligotrophic surface layer overlies a nutrient-rich eutrophic deeper layer (Herbland and Voituriez, 1979; Small *et al.*, 1987). Such a pattern has been often observed in the western Pacific at 165°E (Radenac and Rodier, 1996) and 155°E (Mackey *et al.*, 1995), and is associated with "warm pool waters". However, the eastward extension of this depleted layer as far as 173°W was anomalous, as shown by a comparison with climatology. Figure 6 presents nitrate and phosphate anomalies relative to the NOAA Atlas climatology; silicate climatology is poor in the 180°–170°W area, preventing computation of anomalies. Surface nitrate and phosphate anomalies (Fig. 6a) were always negative, with maximum values (2.5 μM and 0.35 μM, respectively) observed from the Date Line to the eastern limit of the oligotrophic system. West of the Date Line, the westward decrease of surface anomalies reflected the westward decrease of nutrient climatology caused by objective analysis, whereas cruise values stayed close to zero. East of the salinity front surface concentrations were only slightly less than climatology, except in the 162–156°W zone of nutrient minima. At the depth of the nitracline (110–130 dbar), positive nitrate anomalies of 4–5 μM were noticeable. Between the Date Line and 160°W, concentrations were about normal, and east of that longitude appeared negative anomalies of 2 μM. Like the thermocline (Fig. 3b), the nitracline was shallower than normal in the west, and deeper than normal in the east.

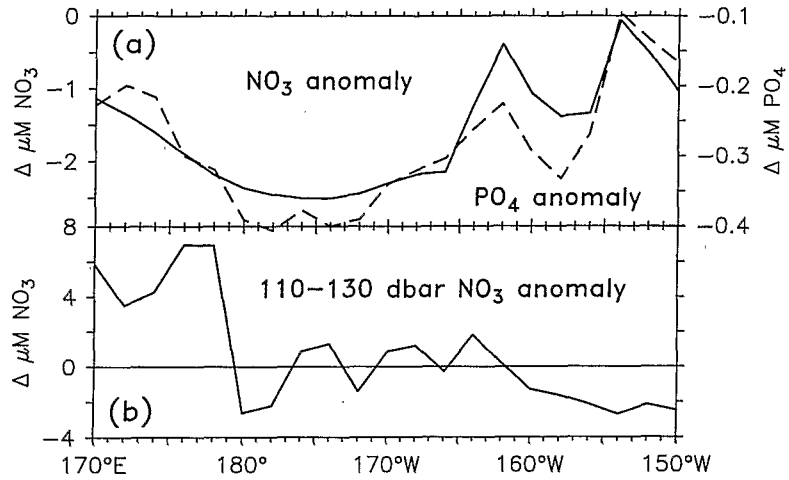

Fig. 6. (a) Surface nitrate (continuous line) and phosphate (dashed line) concentrations and (b) nitrate concentration anomaly at the top of the nitracline.

DISCUSSION OF MECHANISMS INVOLVED

Large-scale context

To understand the mechanisms producing the observed anomalies in the physical and nutrient structures, it is essential to replace the FLUPAC measurements in the large-scale context of the tropical Pacific at the end of 1994. Satellite data and observation networks have shown that, from July to December 1994, a series of surface warming events at intraseasonal time-scale have taken place, associated with strong westerly wind bursts in the west and propagation of Kelvin waves throughout the Pacific (Liu *et al.*, 1995). Whether these events have led to a full-fledged El Niño event is still unclear, but they may be responsible for some of our observations. Zonal wind and current data at 10 m depth from a mooring at 0°–165°E (P. Freitag, personal communication, 1996) (Fig. 7) show that, beginning in September 1994, several westerly wind bursts with a period of 30–40 days occurred at 165°E. They were manifestations of the Madden–Julian atmospheric oscillation (Madden and Julian, 1972), which penetrates to the western Pacific from the Indian Ocean. The first strong wind burst began on 6 September and lasted for 11 days, with an average zonal wind of 4.8 m s^{-1}. It had been preceded by 50 days of weaker westerly winds of average speed 2.9 m s^{-1}, so that winds were generally westerlies at 165°E throughout the 15 July–16 September period except for a few days of calm. The wind fetch extended to at least from 150° to 170°E on a 2°N–2°S average (Fig. 8a). The upper ocean immediately reacted and, at 165°E, an eastward current jet developed on 16 July, which lasted until 24 September, with an average zonal speed of 0.39 m s^{-1} (Fig. 7b). Kessler *et al.* (1995) noted that episodes of eastward penetration of the Madden–Julian oscillation are connected to generation of downwelling Kelvin waves (DKW) that propagate eastward at a phase speed of about 2.3 m s^{-1}. The first evidence is given by a time–longitude plot of zonal wind field and depth of the thermocline, obtained from the TAO array (Fig. 8): westerly episodes of July, September, November and December 1994 were followed by depressions of the thermocline of the order of 10–20 m, which propagated eastward from the easternmost

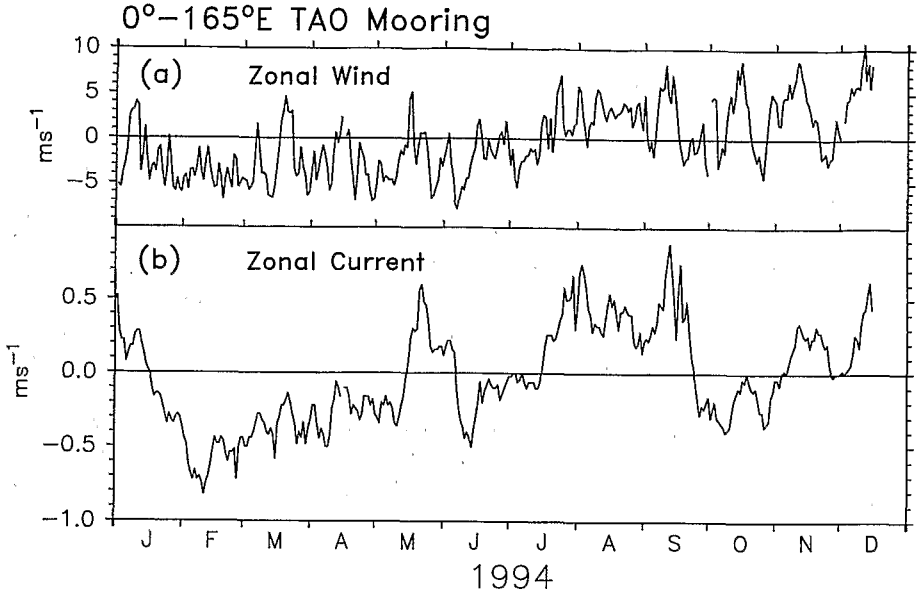

Fig. 7. (a) Zonal wind at 3 m height and (b) ADCP zonal current at 14 m depth from the 0°–165°E TAO mooring.

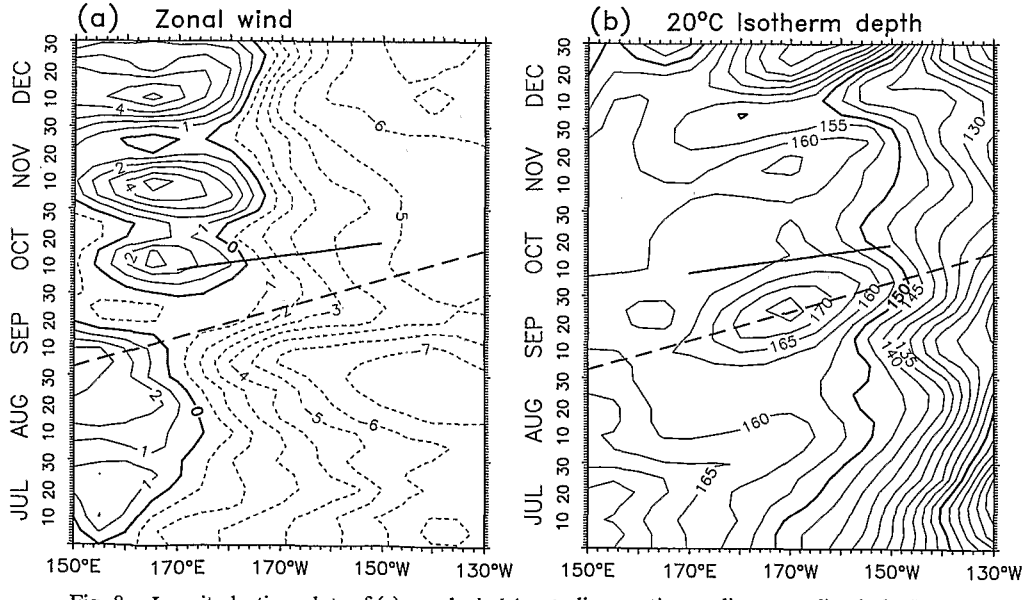

Fig. 8. Longitude–time plots of (a) zonal wind (westerlies, continuous line; easterlies dashed) and (b) 20°C isotherm depth from the TAO array. FLUPAC cruise track (continuous line) and Kelvin wave ray path for a 2.3 m s^{-1} propagation (dashed line) are superimposed. TAO data courtesy of M. McPhaden, Director, TAO Project Office.

extension of the westerly winds as signatures of DKWs. Generation and propagation of these particular Kelvin waves were recently confirmed by another study based on TOPEX–POSEIDON altimeter data and model computations (Boulanger and Fu, 1996). An exception was the 10–20 October westerly burst, which did not seem to trigger a wave. Linear theory of equatorial waves predicts that wave amplitude is proportional to wind fetch, duration and wind speed squared, so that a Kelvin wave triggered by the relatively limited October burst may have been below the limit of detection of TAO measurements.

In the eastern part of the section, TAO data also showed a moderate activity of Tropical Instability Waves (TIW). A time series of 0–500 dbar dynamic height at 5°N and the equator for 3 years shows distinct periodic oscillations (Fig. 9). These non-linear waves, triggered by high meridional shear of zonal currents, are characterized by meridional oscillations with a period of 20–30 days and wavelengths of the order of 1000 km, and propagate westward at about 0.5 m s^{-1} (e.g. Qiao and Weisberg, 1995). In terms of thermal structure variations, TIW activity is usually maximum away from the equator. At the end of 1994, at 155°W, activity was lower at 5°N than in other years, but on the equator, TIW activity was similar to that in other years, although other time-scales of variability were also visible in the dynamic height signal.

Along the FLUPAC track

The FLUPAC cruise reached 170°E on 9 October, 2 weeks after the end of the eastward jet at 165°E. In this area, the zonal extension of warm pool waters is mostly governed by anomalous zonal advection, at time-scales of several months (Picaut and Delcroix, 1995).

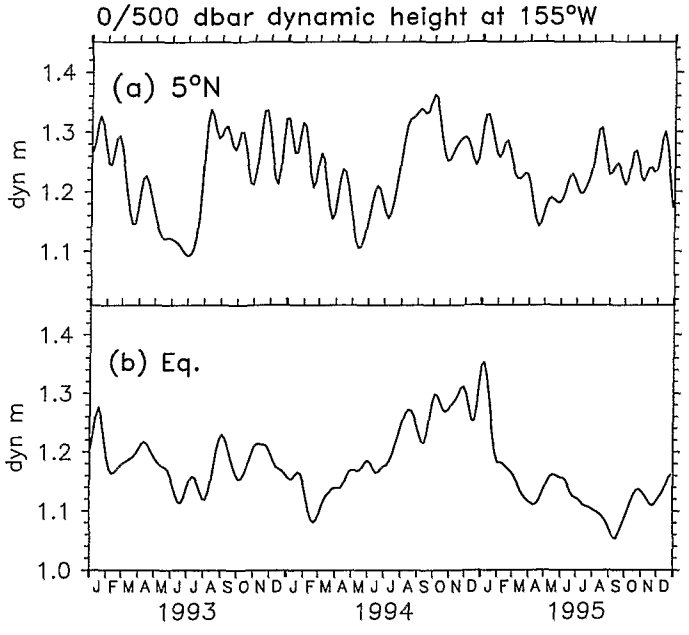

Fig. 9. The 0–500 dbar time series of dynamic height from the TAO moorings at 155°W, (a) at 5°N, (b) on the equator, for the period 1993–1995. Tropical instability wave activity is apparent.

We hypothesize that advection is still of major importance at our shorter time-scales: in this case, the above-mentioned jet would have caused an eastward displacement of about 2400 km of surface isolines (0.39 m s^{-1} times 71 days, i.e. 2392 km). Assuming that distribution of nutrients was close to climatology before the westerly winds of July–September (i.e. the 1 μM nitrate and 0.2 μM phosphate isolines at 170°E), the zonal position of the 1 μM nitrate isoline (165°W, 2800 km to the east) or the 0.2 μM phosphate isoline (167°W, 2600 km to the east) agrees well with that advective hypothesis. The existence of an important barrier layer at the base of that water mass prevented enrichment from vertical mixing along its displacement. It is more difficult to calculate the zonal displacement for temperature because of the homogeneity of the temperature field and local heat exchange with the atmosphere, which plays an important role at these short time-scales. The position of the salinity front cannot be obtained from the climatology, where frontal features are blurred by definition. However, as cited above, previous work had shown this front to be located about 20° to the west of its position during FLUPAC. An eastward displacement of 20° (2200 km) also would be in agreement with the zonal advection hypothesis. Yet, at the time of FLUPAC the observed flow had mostly returned to westward, west of the front, for which a tentative explanation will be given below. The small patch of eastward flow subsisting from 180–172°W was a last remnant of the eastward jet of the previous weeks.

The FLUPAC track (continuous line) is superimposed on the thermocline depth plot (Fig. 8b), and shows that the cruise closely followed the bulk of the DKW triggered by the September wind burst (dashed line), and was nearest the maximum associated thermocline depression at 165–160°W. The progressive approach of that DKW explains the deepest position of the thermocline found at the same longitude during FLUPAC. That DKW also was associated with a positive sea-level swelling on the equator, which means an eastward geostrophic current field that travelled with the wave (Delcroix *et al.*, 1991). The eastward zonal component observed above the thermocline where the DKW influence was maximum (east of 170°W) was a manifestation of that geostrophic flow. The presence of that sea-level anomaly and eastward, convergent surface flow would have at least temporarily balanced the wind-driven Ekman divergence responsible for equatorial upwelling under a trade wind regime. Indeed, meridional temperature sections obtained from the TAO moorings along 155°W in the last week of September (not shown) present an inverted meridional curvature of isotherms 27–28°C around the equator, indicative of actual downwelling. This was the time of arrival of the DKW "crest" at that longitude, and that downwelling coincided with the deepening of the thermocline (Fig. 8b). Also, secondary surface temperature maximum at 160–156°W, horizontal intrusive *T–S* structures under 50 m and nutrient minima at 162–158°W were signs of absence of vertical advection there. However, strong upwelling must have been present about 1 month before, when strong trade winds existed to the west of 170°W (Fig. 8a), and nutrients were still present in this well-mixed layer. The inversion in zonal slope of the thermocline is also a consequence of the advection of warm water and propagation of the DKW, which resulted in uplifting of thermocline isotherms in the western part of the transect. The nitracline was consequently uplifted in the area, and blocking by the barrier layer above explained the high vertical nitrate gradient.

Activity of TIWs was maximum in the area east of the salinity front, and the associated meridional advection may explain the spreading of upper thermocline isotherms, as already noted by Kessler and McPhaden (1995). In the same way, the nutrient-depleted region at 162–158°W coincided with the strongest meridional advection, mostly from the north.

Strong modifications of the shear-driven mixing east of the salinity front were probably the consequence of wave activity. The effects of instability waves that should lead to an increase of the vertical shear because of enhancement of the meridional component (Peters *et al.*, 1991) were counteracted by the effects of the DKW that resulted in a very low vertical shear: eastward flow associated with the DKW extended from the surface to the EUC. The overall vertical shear above the EUC was much lower than generally reported, leading to an unusually low turbulent regime; in these conditions, surface waters could not be rapidly re-enriched through vertical turbulent mixing.

Equatorially trapped wave dynamics also may have played a role in the extreme western part of the section, west of the Date Line, where strong westward surface currents were opposed to the local wind. Sea-level anomaly data from the TOPEX–POSEIDON satellite, projected onto first Rossby modes of a linear model, show that an upwelling Rossby wave triggered by the strong trade winds of the central Pacific would have arrived west of the Date Line at the time of FLUPAC (Boulanger and Fu, 1996). This type of wave presents only a small signature in thermocline shoaling right on the equator and is not readily observable in available mooring data. However, it has a westward geostrophic velocity field that would be coherent with our observations of westward flow at 170–180°E, opposed to the local wind forcing. An exact computation of the geostrophic velocity from the wave amplitude curvature at the equator is not possible at these short time scales.

CONCLUSIONS

One leg of the FLUPAC cruise carried out along the Pacific equator from 170°E to 150°W in October 1994 provided a description of the effects of a strong westerly wind burst on the physical and nutrient structures that could be explained only with the help of large-scale data from the TAO array. In the western part of the section, zonal advection was dominant at the surface: the eastward current jet triggered by the burst transported nutrient-depleted warm pool waters eastward. Because of a thick barrier layer above the thermocline vertical mixing was prevented, and these waters kept their characteristics along their path. Below the surface layer, nutrient vertical gradients were enhanced. In the east, propagation of a downwelling Kelvin wave caused a depression of the thermocline and nitracline, and temporarily stopped upwelling. Despite the presence of tropical instability wave activity, vertical mixing does not replenish surface waters with nutrients: the velocity field associated with the Kelvin waves decreases vertical velocity shear and turbulence.

Effects of a single strong westerly wind burst in the western equatorial Pacific have thus propagated eastward through different mechanisms, leading to a nutrient depletion or a cessation of enrichment of upper ocean waters along the equator. To completely understand how these effects could influence primary production and biology, a knowledge of their evolution in time would be necessary, which cannot be obtained from cruise nutrient data alone. Time series of nutrient measurements would probably be as useful as time-series of physical variables are.

Acknowledgements—Financial support for this work was provided by INSU–CNRS and ORSTOM. The assistance of officers and crew of R.V. *L'Atalante* of IFREMER during the FLUPAC cruise was much appreciated. Sylvain Bonnet, Philippe Gérard and Hugues Lemonnier performed round-the-clock chemical analyses, Francis Gallois and Jean-Yves Panché provided much needed technical help. This paper is dedicated to the memory of Sylvain.

REFERENCES

Bahr, F., Firing, E. and Jiang, S. (1989) Acoustic Doppler current profiling in the western Pacific during the US-PRC TOGA cruises 2, 3 and 4. JIMAR Data Report 5, University of Hawaii, 199 pp.

Barber, R. T. and Chavez, F. P. (1983) Biological consequences of El Niño. *Science*, **222**, 1203–1210.

Barber, R. T. and Kogelschatz, J. E. (1990) Nutrients and productivity during the 1982/83 El Niño. In *Global Ecological Consequences of the 1982–83 El Niño–Southern Oscillation*, P. W. Glynn (ed.), pp. 21–53, Amsterdam.

Blanchot, J., Rodier, M. and Le Bouteiller, A. (1992) Effect of El Niño–Southern Oscillation events on the distribution and abondance of phytoplankton in the western Pacific Ocean along 165°E. *Journal of Plankton Research*, **4**, 137–156.

Bonnet, S. (1995) Manuel d'analyses chimiques dans l'eau de mer. Notes Techniques Sciences de la Mer; Océanographie 2, 40 pp. ORSTOM, Nouméa.

Boulanger, J.-P. and Fu, L. L. (1996) Evidence of boundary reflection of Kelvin and first-mode Rossby waves from TOPEX/POSEIDON sea level data. *Journal of Geophysical Research*, **101**, 16361–16371.

Carr, M. E., Oakey, N. S., Jones, B. and Lewis, M. R. (1992) Hydrographic patterns and vertical mixing in the equatorial Pacific along 150°W. *Journal of Geophysical Research*, **97**, 611–626.

Conkright, M. E., Levitus, S. and Boyer, T. P. (1994) *World Ocean Atlas 1994, Vol. 1: Nutrients*. NOAA Atl. NESDIS 1, Washington, DC, 150 pp.

Dandonneau, Y. (1992) Surface chlorophyll concentration in the tropical Pacific ocean: an analysis of data collected by merchant ships from 1978 to 1989. *Journal of Geophysical Research*, **97**, 3581–3591.

Delcroix, T., Eldin, G., McPhaden, M. and Morlière, A. (1993) Effects of westerly wind bursts upon the western equatorial Pacific Ocean, February–April 1991. *Journal of Geophysical Research*, **98**, 16379–16385.

Delcroix, T., Eldin, G., Radenac, M.-H., Toole, J. and Firing, E. (1992) Variation of the western equatorial Pacific Ocean, 1986-1988. *Journal of Geophysical Research*, **97**, 5423–5446.

Delcroix, T., Picaut, J. and Eldin, G. (1991) Equatorial Kelvin and Rossby waves evidenced in the Pacific Ocean through GEOSAT sea-level and surface current anomalies. *Journal of Geophysical Research, Supplement*, **96**, 3249–3262.

Eldin, G., Delcroix, T., Hénin, C., Richards, K., du Penhoat, Y., Picaut, J. and Rual, P. (1994) Large-scale current and thermohaline structures along 156°E during the COARE Intensive Observation Period. *Geophysical Research Letters*, **21**, 2681–2684.

Eldin, G., Morlière, A. and Reverdin, G. (1992) Acoustic Doppler current profiling along the Pacific equator from 95°W to 165°E. *Geophysical Research Letters*, **19**, 913–916.

Enfield, D. B. (1987) The intraseasonal oscillation in eastern Pacific sea-levels: How is it forced? *Journal of Physical Oceanography*, **17**, 1860–1876.

Feely, R. A., Gammon, R. H., Taft, B. A., Pullen, P. E., Waterman, L. S., Conway, T. J., Gendron, J. F. and Wisegarver, D. P. (1987) Distribution of chemical tracers in the eastern equatorial Pacific during and after the 1982–1983 El Niño–Southern Oscillation event. *Journal of Geophysical Research*, **92**, 6545–6558.

Firing, E. (1987) Deep zonal currents in the central equatorial Pacific. *Journal of Marine Research*, **45**, 791–812.

Halpern, D. (1980) A Pacific equatorial temperature section from 172°E to 110°W during winter and spring 1979. *Deep-Sea Research*, **27A**, 931–940.

Herbland, A. and Voituriez, B. (1979) Hydrological structure analysis for estimating the primary production in the tropical Atlantic Ocean. *Journal of Marine Research*, **37**, 87–101.

JGOFS (1990) Report of a Workshop on Equatorial Pacific Process Studies, Tokyo, April 1990. Report 8, JGOFS, 75 pp. Scientific Committee for Ocean Research, Halifax.

Johnson, E. S. and Luther, D. S. (1994) Mean zonal momentum balance in the upper and central equatorial Pacific Ocean. *Journal of Geophysical Research*, **99**, 7689–7705.

Kessler, W. S. and McPhaden, M. J. (1995) The 1991–1993 El Niño in the central Pacific. *Deep-Sea Research II*, **42**, 295–333.

Kessler, W. S., McPhaden, M. J. and Weickmann, K. M. (1995) Forcing of intraseasonal Kelvin waves in the equatorial Pacific. *Journal of Geophysical Research*, **100**, 10613–10631.

Kessler, W. S. and Taft, B. A. (1987) Dynamic heights and zonal geostrophic transports in the central tropical Pacific during 1979–84. *Journal of Physical Oceanography*, **17**, 97–122.

Kuroda, Y. and McPhaden, M. J. (1993) Variability in the western equatorial Pacific Ocean during Japanese Pacific climate study cruises in 1989 and 1990. *Journal of Geophysical Research*, **98**, 4747–4759.

Le Borgne, R., Brunet, C., Eldin, G., Radenac, M.-H. and Rodier, M. (1995) Campagne océanographique

FLUPAC à bord du N.O. *L'Atalante*, 23 septembre au 29 octobre 1994, recueil des données, Tome 1. *Archives Sciences de la Mer, Oceanographie 1*, ORSTOM, Nouméa, 337 pp.

Le Bouteiller, A., Blanchot, J. and Rodier, M. (1992) Size distributions patterns of phytoplankton in the western Pacific: towards a generalization for the tropical open ocean. *Deep-Sea Research*, **39**, 805–823.

Lien, R.-C., Caldwell, D. R., Gregg, M. C. and Moum, J. N. (1995) Turbulence variability at the equator in the central Pacific at the beginning of the 1991–93 El Niño. *Journal of Geophysical Research*, **100**, 6881–6898.

Liu, W. T., Tang, W. and Fu, L.-L. (1995) Recent warming event in the Pacific may be an El Niño. *EOS, Transactions, American Geophysical Union*, **76**, 429.

Lukas, R. and Lindstrom, E. (1991) The mixed layer of the western equatorial Pacific Ocean. *Journal of Geophysical Research*, **96** (Suppl.), 3343–3357.

Mackey, D. J., Parslow, J., Higgins, H. W., Griffiths, F. B. and O'Sullivan, J. E. (1995) Plankton productivity and biomass in the western equatorial Pacific: biological and physical controls. *Deep-Sea Research II*, **42**, 499–553.

Madden, R. A. and Julian, P. R. (1972) Description of global-scale circulation cells in the tropics with a 40–50 day period. *Journal of Atmospheric Science*, **29**, 1109–1123.

Mangum, L. J., Hayes, S. P., Toole, J. M., Wang, Z., Pu, S. and Hu, D. H. (1990) Thermohaline structure and zonal pressure gradient in the western equatorial Pacific. *Journal of Geophysical Research*, **95**, 7279–7288.

McCarty, M. E. and McPhaden, M. J. (1993) Mean seasonal cycles and interannual variations at 0°, 165°E during 1986–1992. NOAA Technical Memo., ERL PMEL 98, NOAA, Washington, DC, 64 pp.

McPhaden, M. J., Freitag, P., Hayes, S., Taft, B., Chen, Z. and Wyrtki, K. (1988) The response of the equatorial Pacific Ocean to a westerly wind burst in May 1986. *Journal of Geophysical Research*, **93**, 10589–10603.

McPhaden, M. J., Hayes, S. P., Mangum, L. J. and Toole, J. (1990) Variability in the western equatorial Pacific during the 1986–87 El Niño/Southern Oscillation event. *Journal of Physical Oceanography*, **20**, 190–208.

Murray, J. W., Johnson, E. and Garside, E. (1995) A US JGOFS process study in the equatorial Pacific (EqPac): Introduction. *Deep-Sea Research II*, **42**, 275–293.

Oudot, C. and Montel, Y. (1988) A high sensitivity method for the determination of nanomolar concentrations of nitrate and nitrite in sea-water with a Technicon Autoanalyzer II. *Marine Chemistry*, **24**, 239–252.

Peters, H., Gregg, M. C. and Sanford, T. B. (1991) Equatorial and off-equatorial fine-scale and large-scale shear variability at 140°W. *Journal of Geophysical Research*, **96**, 16913–16928.

Picaut, J. and Delcroix, T. (1995) Equatorial wave sequence associated with Warm Pool displacements during the 1986–1989 El Niño–La Niña. *Journal of Geophysical Research*, **100**, 18393–18408.

Qiao, L. and Weisberg, R. H. (1995) Tropical instability waves kinematics: observations from the Tropical Instability Wave Experiment. *Journal of Geophysical Research*, **100**, 8677–8694.

Radenac, M.-H. and Rodier, M. (1996) Nitrate and chlorophyll distributions in relation to thermohaline and current structures in the western tropical Pacific during 1985–89. *Deep-Sea Research II*, **43**, 725–752.

Small, L. F., Knauer, G. A. and Tuel, M. D. (1987) The role of sinking fecal pellets in stratified euphotic zones. *Deep-Sea Research*, **34**, 1705–1712.

Strickland, J. and Parsons, T. (1972) *A Practical Handbook of Seawater Analysis*. Fisheries Research Board of Canada, 167, Ottawa, 310 pp.

Tsuchiya, M., Lukas, R. and Fine, R. A. (1989) Source waters of the Pacific equatorial undercurrent. *Progress in Oceanography*, **23**, 101–147.

Weisberg, R. H. and Hayes, S. P. (1995) Upper ocean variability on the equator in the Pacific at 170°W. *Journal of Geophysical Research*, **100**, 20485–20498.

Wijesekera, H. W. and Gregg, M. C. (1996) Surface layer response to weak winds, westerly bursts, and rain squalls in the western Pacific Warm Pool. *Journal of Geophysical Research*, **101**, 977–997.

Wilson, D. and Leetmaa, A. (1988) Acoustic Doppler current profiling in the equatorial Pacific in 1984. *Journal of Geophysical Research*, **93**, 13947–13966.